2006-1

An Explicit Scheme for Multifluid Magnetohydrodynamics

Stephen O'Sullivan
Technological University Dublin, stephen.osullivan@tudublin.ie

Turlough Downes
Dublin City University

An explicit scheme for multifluid magnetohydrodynamics

Stephen O'Sullivan[1]⋆ and Turlough P. Downes[2]⋆

[1]*UCD School of Mathematical Sciences, University College Dublin, Belfield, Dublin 4*
[2]*School of Mathematical Sciences, Dublin City University, Glasnevin, Dublin 9*

ABSTRACT

When modelling astrophysical fluid flows, it is often appropriate to discard the canonical magnetohydrodynamic approximation, thereby freeing the magnetic field to diffuse with respect to the bulk velocity field. As a consequence, however, the induction equation can become problematic to solve via standard explicit techniques. In particular, the Hall diffusion term admits fast-moving whistler waves which can impose a vanishing time-step limit.

Within an explicit differencing framework, a multifluid scheme for weakly ionized plasmas is presented which relies upon a new approach to integrating the induction equation efficiently. The first component of this approach is a relatively unknown method of accelerating the integration of parabolic systems by enforcing stability over large compound time-steps rather than over each of the constituent substeps. This method, Super Time-Stepping, proves to be very effective in applying a part of the Hall term up to a known critical value. The excess of the Hall term above this critical value is then included via a new scheme for pure Hall diffusion.

Key words: MHD – shock waves – methods: numerical – ISM: clouds – dust, extinction.

1 INTRODUCTION

Dynamically important magnetic fields are commonplace in astrophysics. In many cases, where these fields interact with fluids, researchers have assumed that the equations of ideal magnetohydrodynamics (MHD) are sufficient in modelling the evolution of the magnetic fields and the fluids with which they interact. There are clear examples, however, where the assumptions underpinning the equations of ideal MHD are not valid. In dense molecular clouds, for example, the density of charged particles can be much lower than that of the neutral species (Ciolek & Roberge 2002, hereafter CR02). Under these conditions, coupling between the motions of the fluids and the magnetic field is not perfect, and diffusive effects become significant. Similarly, ideal MHD is not believed to be valid in accretion discs around young stellar objects (Wardle 2004). The latter point is particularly interesting given the importance attached to the interaction between accretion discs and magnetic fields in the launching of stellar jets and outflows (e.g. Shu et al. 1994; Fendt & Camenzind 1996; Ouyed, Pudritz & Stone 1997; Lery et al. 1999; Ferreira 2004). When modelling systems such as these therefore, a full multifluid treatment permitting relative motions between different component species should be adopted.

Many authors (Tóth 1994; Smith & Mac Low 1997; Stone 1997; Chieze, Pineau des Forets & Flower 1998) have suggested schemes for numerically integrating the multifluid equations in the limit of pure ambipolar diffusion. In this regime, the charged species are

firmly tied to the magnetic field lines as they diffuse through the neutral gas. The problem becomes more technically challenging, however, when charged species may be loosely attached to the field lines and Hall diffusion can become important. Notably, it is thought that Hall diffusion may play an important role in environments such as the surfaces of neutron stars (Hollerbach & Rüdiger 2004), protostellar discs (Wardle 2004) and dense molecular clouds (CR02).

In their numerical studies of molecular clouds, CR02 assumed that the ionization fraction is low and that the inertia of the charged particles may be neglected. They were then able to integrate the governing equations for a multifluid problem including the presence of several species of charge-carrying grain. Separately, Sano & Stone (2002a,b) performed multifluid calculations designed to examine the Hall effect in the context of the magnetorotational instability in accretion discs. However, both of the schemes used by these authors are subject to a rather stringent stability criterion which requires that the time-step tends to zero as the Hall effect becomes large Falle (2003, hereafter F03). To circumvent this constraint F03 presents a scheme employing an implicit method of integrating the magnetic field equation. This has the advantage of allowing time-steps up to the limit dictated by the hyperbolic components of the equations. However, since large-scale multifluid simulations are of obvious interest, the inherent difficulty of parallelizing implicit schemes becomes a serious disadvantage.

In this work, we present a fully explicit numerical scheme for solving the multifluid equations describing a weakly ionized plasma. The usual stability restrictions are relaxed through a combination of a technique known as Super Time-Stepping (STS) (Alexiades, Amiez & Gremaud 1996) and a new method which we call the Hall

---

⋆E-mail: stephen.osullivan@ucd.ie (SOS); turlough.downes@dcu.ie (TPD)

diffusion scheme (HDS). Crucially, since the scheme is explicit, it is straightforward to parallelize and to implement on top of an adaptive mesh refinement (AMR) engine.

In Section 2, the governing equations are described; Section 3 contains a detailed description and analysis of the numerical scheme; Section 4 contains numerical tests demonstrating the reliability of the scheme and in Section 5, the relevance of this work is discussed.

2 THE MULTIFLUID EQUATIONS

We assume a weakly ionized plasma such that the mass density is dominated by the neutral component of the gas. Then, relative to the scalelength of the system, if particles of a given charged species have small mean free paths in the neutral gas, or small Larmor radii, their pressure and inertia may be neglected.

For convenience it is assumed there is no mass transfer between species. It is straightforward, however, to insert the necessary terms for a more general treatment to include mass transfer (for example, see F03 and CR02) if desired. The equations governing the evolution of the multifluid system (CR02; F03) can then be written as

$$\frac{\partial \rho_i}{\partial t} + \frac{\partial}{\partial x}(\rho_i \boldsymbol{q}_i) = 0, \tag{1}$$

$$\frac{\partial \rho_1 \boldsymbol{q}_1}{\partial t} + \frac{\partial}{\partial x}(\rho_1 u_1 \boldsymbol{q}_1 + p_1 \mathsf{I}) = \boldsymbol{J} \times \boldsymbol{B}, \tag{2}$$

$$\frac{\partial e_1}{\partial t} + \frac{\partial}{\partial x}\left[u_1\left(e_1 + p_1 + \frac{1}{2}\rho_1 q_1^2\right)\right] = \boldsymbol{J} \cdot \boldsymbol{E} + \sum_{i=1}^{N} H_i, \tag{3}$$

$$\frac{\partial \boldsymbol{B}}{\partial t} + \frac{\partial \boldsymbol{M}}{\partial x} = \frac{\partial}{\partial x}\mathsf{R}\frac{\partial \boldsymbol{B}}{\partial x}, \tag{4}$$

$$\alpha_i \rho_i (\boldsymbol{E} + \boldsymbol{q}_i \times \boldsymbol{B}) + \rho_i \rho_1 K_{i1}(\boldsymbol{q}_1 - \boldsymbol{q}_i) = 0, \tag{5}$$

$$H_i + G_{i1} + \alpha_i \rho_i \boldsymbol{q}_i \cdot \boldsymbol{E} = 0, \tag{6}$$

$$\frac{\partial B_x}{\partial x} = 0, \tag{7}$$

$$\sum_{i=2}^{N} \alpha_i \rho_i = 0, \tag{8}$$

$$\sum_{i=2}^{N} \alpha_i \rho_i \boldsymbol{q}_i = \boldsymbol{J}. \tag{9}$$

The subscripts denote the species, with a subscript of 1 indicating the neutral fluid. The variables ρ_i, $\boldsymbol{q}_i \equiv (u_i, v_i, w_i)^{\mathrm{T}}$ and p_i are the mass density, velocity and pressure of species i. The identity matrix, current density and magnetic flux density are represented by I, $\boldsymbol{J}$, $\boldsymbol{B}$ respectively. K_{i1} describes the collisional interaction between species i and the neutral fluid, α_i is the charge-to-mass ratio for species i, G_{i1} is the energy transfer rate from species i to the neutral fluid, H_i is the energy source or sink appropriate to species i, R is the resistivity matrix and $\boldsymbol{M}$ is the hyperbolic flux of $\boldsymbol{B}$. See F03 and CR02 for a more detailed description of these terms. Note that in general K_{i1} and G_{i1} may depend on the temperatures

and relative velocities of the interacting species. Equations (1)–(6) are the equations governing the conservation of mass, neutral momentum, neutral energy, magnetic flux, charged momentum and charged energy. Equations (7)–(9) describe the divergence of $\boldsymbol{B}$, charge neutrality and current, respectively.

From Faraday's law in one dimension $\partial B_x / \partial t = 0$ so that the trivial B_x component may be dropped from equation (4). The hyperbolic flux is then

$$\boldsymbol{M} = (u_1 B_y - v_1 B_x, u_1 B_z - w_1 B_x), \tag{10}$$

and the resistivity matrix is

$$\mathsf{R} = \begin{pmatrix} (r_{\mathrm{O}} - r_{\mathrm{A}})\frac{B_z^2}{B^2} + r_{\mathrm{A}} & (r_{\mathrm{A}} - r_{\mathrm{O}})\frac{B_y B_z}{B^2} + r_{\mathrm{H}}\frac{B_x}{B} \\ (r_{\mathrm{A}} - r_{\mathrm{O}})\frac{B_y B_z}{B^2} - r_{\mathrm{H}}\frac{B_x}{B} & (r_{\mathrm{O}} - r_{\mathrm{A}})\frac{B_y^2}{B^2} + r_{\mathrm{A}} \end{pmatrix}, \tag{11}$$

where r_{O}, r_{H} and r_{A} are the Ohmic, Hall and ambipolar resistivities, respectively, and are defined by

$$r_{\mathrm{O}} = \frac{1}{\sigma_{\mathrm{O}}}, \tag{12}$$

$$r_{\mathrm{H}} = \frac{\sigma_{\mathrm{H}}}{\sigma_{\mathrm{H}}^2 + \sigma_{\mathrm{A}}^2}, \tag{13}$$

$$r_{\mathrm{A}} = \frac{\sigma_{\mathrm{A}}}{\sigma_{\mathrm{H}}^2 + \sigma_{\mathrm{A}}^2}, \tag{14}$$

with conductivities

$$\sigma_{\mathrm{O}} = \sum_{i=2}^{N} \alpha_i \rho_i \beta_i, \tag{15}$$

$$\sigma_{\mathrm{H}} = \frac{1}{B}\sum_{i=2}^{N} \frac{\alpha_i \rho_i}{1 + \beta_i^2}, \tag{16}$$

$$\sigma_{\mathrm{A}} = \frac{1}{B}\sum_{i=2}^{N} \frac{\alpha_i \rho_i \beta_i}{1 + \beta_i^2}, \tag{17}$$

where the Hall parameter for species i is given by

$$\beta_i = \frac{\alpha_i \boldsymbol{B}}{K_{1i}\rho_1}. \tag{18}$$

3 NUMERICAL APPROACH

3.1 The gas equations

Assuming a piecewise-constant solution at time t^n on a uniform mesh of spacing h, the solution at a later time $t^{n+1} = t^n + \tau$ is sought. The state in cell j represents the volume average over $(j - 1/2)h \leqslant x \leqslant (j + 1/2)h$.

It should first be noted that the charged particle pressures[1] and velocities (p_i^{n+1} and $\boldsymbol{q}_i^{n+1}$ for $i > 1$) can be obtained algebraically through equations (5) and (6). This procedure is described in Appendix A.

---

[1] It is actually temperatures of the charged species which are derived as their pressures are not explicitly necessary under the assumptions made here.

To obtain the full solution at time t^{n+1}, finite volume methods are applied to equations (1)–(8). The time integration is multiplicatively operator split into five operations, with each carried out to second-order accuracy in space and time. The order is permuted over successive time-steps such that second-order temporal accuracy is maintained over the full step (Strang 1968). In the following, the five necessary operations for finite volume integration are described.

(i) Equations (1)–(3) (with $i = 1$ for the mass equation) form a system of equations for the neutral gas. Working in terms of the primitive variables $\boldsymbol{P} = (\rho_1, \boldsymbol{q}_1, p_1)^{\mathrm{T}}$, fluxes are evaluated from a piecewise-constant solution $\boldsymbol{P}^n$ via a hydrodynamic Riemann solver. A time-centred solution, $\boldsymbol{P}^{n+1/2}$, obtained from these fluxes is then reconstructed to a second-order piecewise-linear solution, $\bar{\boldsymbol{P}}^{n+1/2}$, using van Albada non-linear averaging for the gradients. Fluxes may then be derived from $\bar{\boldsymbol{P}}^{n+1/2}$ which are second-order accurate in space and time (for further details see, for example, Falle 1991). These fluxes are then applied to the conserved variables.

(ii) The source terms on the right-hand sides of equations (2) and (3) are applied.

(iii) The charged particle mass fluxes are applied using equation (1) with $i > 1$ in a second-order upwind procedure similar to that used for the neutral gas.

(iv) The hyperbolic flux on the left-hand side of equation (4) is applied via a centred approximation

$$\boldsymbol{M}_{j+1/2} = \frac{1}{2}(\boldsymbol{M}_{j+1} + \boldsymbol{M}_j). \tag{19}$$

This has the disadvantage of not coupling the bulk fluid to the magnetic field through a Riemann problem, however, it is necessary in order that purely hydrodynamic subshocks may be properly captured. As remarked by F03, as long as the magnetic field appears continuous on the grid, as should be the case with finite resistivities, this is perfectly acceptable.

(v) The resistive term on the right-hand side of equation (4) is applied. Discussion of this procedure is deferred to the following section since it is of special interest.

3.2 Magnetic diffusion

Splitting the hyperbolic flux term $\partial \boldsymbol{M}/\partial x$ from the induction equation (4) and linearizing yields

$$\frac{\partial \boldsymbol{B}}{\partial t} = \mathbf{R}\frac{\partial^2 \boldsymbol{B}}{\partial x^2}. \tag{20}$$

Note that the linearized form is assumed for convenience in the following analysis and in practice generalized discretizations of the non-linear diffusion term are used.

3.2.1 Standard discretization

The usual explicit discretization for a diffusion term applied to equation (20) yields

$$\boldsymbol{B}_j^{n+1} = \boldsymbol{B}_j^n + \frac{\tau}{h^2}\mathbf{R}_j^n\left(\boldsymbol{B}_{j+1}^n - 2\boldsymbol{B}_j^n + \boldsymbol{B}_{j-1}^n\right). \tag{21}$$

Assuming r_{O} to be negligible, the relative importance of the remaining resistivities can be parameterized by $\eta \equiv r_{\mathrm{A}}/|r_{\mathrm{H}}|$. F03 showed the above scheme has an amplification matrix with eigenvalues which are real when $\eta \geqslant \eta^*$ and complex otherwise. The

transition point η^* is given by

$$\eta^* = 2|\cos\theta|/\sin^2\theta, \tag{22}$$

where θ is the pitch angle of the field with respect to the x-axis. In the real regime, the stability limit on the time-step is

$$\bar{\tau}^{\mathrm{R}} = \frac{2\sqrt{1+\eta^2}}{\eta(1+\cos^2\theta) + 2|\cos\theta|\sqrt{(\eta/\eta^*)^2 - 1}} \tag{23}$$

where $\bar{\tau} \equiv \tau/\tau^\perp$ and $\tau^\perp$ is the characteristic cell-crossing time for diffusion perpendicular to the magnetic field given by

$$\tau^\perp = \frac{h^2}{2|r_{\mathrm{H}}|\sqrt{1+\eta^2}}. \tag{24}$$

However, below the transition point the stability limit becomes

$$\bar{\tau}^{\mathrm{C}} = \frac{1+\cos^2\theta}{2\cos^2\theta}\frac{\eta}{\sqrt{1+\eta^2}}. \tag{25}$$

In either case the stable time-step limit goes as h^2 since this is an explicit discretization of a diffusion equation, however, a potentially more severe constraint is that while this limit increases as $\eta \to \eta^*$ in the real regime, it rapidly drops to zero as $\eta \to 0$ in the complex regime.

3.2.2 Numerical strategy

Our strategy is to split r_{H} into two parts such that

$$r_{\mathrm{H}} = r_{\mathrm{H}}^a + r_{\mathrm{H}}^b \tag{26}$$

where $r_{\mathrm{H}}^a \equiv \frac{\eta}{\eta^*}r_{\mathrm{H}}$ is the maximum allowable Hall resistivity in the real regime and r_{H}^b is the excess. The induction equation is then integrated in two parts using a technique to accelerate the time-stepping for the standard discretization with Hall resistivity r_{H}^a. The excess Hall resistivity r_{H}^b is then applied using a different discretization with suitable stability properties.

3.2.3 Super Time-Stepping

STS is a technique which can be used to accelerate explicit schemes for parabolic problems. Essentially a Runge–Kutta–Chebyshev method, it has been known for some time (see Alexiades et al. 1996), although it remains relatively unknown in computational astrophysics.

A superstep τ^{STS} is a composite time-step built up from a series of N_{STS} substeps such that

$$\tau^{\mathrm{STS}} = \sum_{j=1}^{N_{\mathrm{STS}}} \mathrm{d}\tau_j. \tag{27}$$

Judicious choice of the $\mathrm{d}\tau_j$ yields stability for the superstep while the normal stability restrictions on the individual substeps are relaxed. Exploiting the properties of Chebyshev polynomials provides a set of optimal values for the substeps given by

$$\mathrm{d}\tau_j = \tau^X\left[(-1+\nu)\cos\left(\frac{2j-1}{N_{\mathrm{STS}}}\frac{\pi}{2}\right) + 1 + \nu\right]^{-1}, \tag{28}$$

where τ^X is the normal explicit time-step limit and ν is a damping factor. Note that $\tau^{\mathrm{STS}} \to N_{\mathrm{STS}}^2\tau^X$ as $\nu \to 0$. The method is unstable in the limit $\nu = 0$. For a more detailed discussion, see Alexiades et al. (1996) and references therein.

In order to apply STS to second order in time Richardson extrapolation is used.

Table 1. Test calculation parameters.

Case A					
Right state	$\rho_1 = 1$	$\boldsymbol{q}_1 = (-1.751, 0, 0)$	$\boldsymbol{B} = (1, 0.6, 0)$	$\rho_2 = 5 \times 10^{-8}$	$\rho_3 = 1 \times 10^{-3}$
Left state	$\rho_1 = 1.7942$	$\boldsymbol{q}_1 = (-0.9759, -0.6561, 0)$	$\boldsymbol{B} = (1, 1.74885, 0)$	$\rho_2 = 8.9712 \times 10^{-8}$	$\rho_3 = 1.7942 \times 10^{-3}$
	$\alpha_2 = -2 \times 10^{12}$	$\alpha_3 = 1 \times 10^8$	$K_{21} = 4 \times 10^5$	$K_{31} = 2 \times 10^4$	$a = 0.1$
	$\nu = 0.05$	$N_{\mathrm{STS}} = 5$	$N_{\mathrm{HDS}} = 0$		
Case B					
Right state	As case A				
Left state	As case A				
	$\alpha_2 = -2 \times 10^9$	$\alpha_3 = 1 \times 10^5$	$K_{21} = 4 \times 10^2$	$K_{31} = 2.5 \times 10^6$	$a = 0.1$
	$\nu = 0$	$N_{\mathrm{STS}} = 1$	$N_{\mathrm{HDS}} = 8$		
Case C					
Right state	$\rho_1 = 1$	$\boldsymbol{q}_1 = (-6.7202, 0, 0)$	$\boldsymbol{B} = (1, 0.6, 0)$	$\rho_2 = 5 \times 10^{-8}$	$\rho_3 = 1 \times 10^{-3}$
Left state	$\rho_1 = 10.421$	$\boldsymbol{q}_1 = (-0.6449, -1.0934, 0)$	$\boldsymbol{B} = (1, 7.9481, 0)$	$\rho_2 = 5.2104 \times 10^{-7}$	$\rho_3 = 1.0421 \times 10^{-2}$
	$\alpha_2 = -2 \times 10^{12}$	$\alpha_3 = 1 \times 10^8$	$K_{21} = 4 \times 10^5$	$K_{31} = 2 \times 10^4$	$a = 1$
	$\nu = 0.05$	$N_{\mathrm{STS}} = 15$	$N_{\mathrm{HDS}} = 0$		

3.2.4 Hall diffusion scheme

Having advanced the induction equation with a Hall resistivity r_{H}^a, it is necessary to find an efficient scheme to impose the excess Hall diffusion r_{H}^b. Since multiplicative operator splitting yields a composite scheme with an amplification factor equal to the product of the amplification factors of the basis schemes this task can be reduced to one of finding a scheme for pure Hall diffusion.

The key observation to make is that $\mathbf{R}$ has zero entries on the diagonal when pure Hall diffusion is being considered. With this in mind, equation (21) may be used to advance one component of the magnetic field explicitly, followed by an implicit-like discretization of the alternate component. We call this the HDS as we are not aware of an instance of this approach elsewhere in the literature. Hence the discretization of equation (21) for the pure Hall excess r_{H}^b becomes

$$B_{yj}^{n+1} = B_{yj}^n + \frac{\tau}{h^2} d_{\mathrm{H}}^b \left(B_{zj+1}^n - 2B_{zj}^n + B_{zj-1}^n \right) \tag{29}$$

followed by

$$B_{zj}^{n+1} = B_{zj}^n - \frac{\tau}{h^2} d_{\mathrm{H}}^b \left(B_{yj+1}^{n+1} - 2B_{yj}^{n+1} + B_{yj-1}^{n+1} \right), \tag{30}$$

where the cosine term is absorbed by defining $d_{\mathrm{H}}^b = r_{\mathrm{H}}^b \cos\theta$. It seems to make little difference which component is advanced first.

For clarity of notation the superscript b is dropped from the following analysis of the stability properties of the scheme. The resistance matrix for pure Hall diffusion is

$$\mathbf{R} = \begin{pmatrix} 0 & d_{\mathrm{H}} \\ -d_{\mathrm{H}} & 0 \end{pmatrix}. \tag{31}$$

Assuming a numerical wave of the form

$$\boldsymbol{B}_j^n = \boldsymbol{B}^n e^{i\omega j} \tag{32}$$

in equations (29) and (30) yields an amplification matrix

$$\mathbf{A} = \begin{pmatrix} 1 & -\hat{d}_{\mathrm{H}} \\ \hat{d}_{\mathrm{H}} & 1 - \hat{d}_{\mathrm{H}}^2 \end{pmatrix}, \tag{33}$$

where $\hat{d}_{\mathrm{H}} \equiv \xi d_{\mathrm{H}}$ and

$$\xi = \frac{2\tau(1 - \cos\omega)}{h^2}. \tag{34}$$

The eigenvalues of $\mathbf{A}$ are given by

$$\lambda = 1 - \frac{1}{2}\hat{d}_{\mathrm{H}}^2 \pm i\frac{1}{2}\hat{d}_{\mathrm{H}}\sqrt{4 - \hat{d}_{\mathrm{H}}^2}, \tag{35}$$

and hence HDS is neutrally stable for $|\hat{d}_{\mathrm{H}}| \leqslant 2$. Taking the most restrictive case of $\omega = \pi$ gives a stable time-step limit of

$$\bar{\tau}^{\mathrm{HDS}} = \frac{\sqrt{1 + \eta^2}}{|\cos\theta|(1 - \eta/\eta^*)}. \tag{36}$$

Note that $\bar{\tau}^{\mathrm{HDS}} \to 1/|\cos\theta|$ as $\eta \to 0$ in contrast to the standard discretization for which $\bar{\tau}^{\mathrm{C}} \to 0$.

The extension of the HDS to more than one dimension is straightforward although we defer a detailed discussion to a later paper. For an outline of the scheme in three dimensions the reader is referred to Appendix B.

In practice, ordinary (unaccelerated) subcycling of HDS, using N_{HDS} subcycles, is applied in conjunction with STS. This compound scheme (referred to as 'STS/HDS' hereafter) usually allows the time-step limit imposed by the hyperbolic terms to be reached efficiently (see Section 4.4).

4 NUMERICAL TESTS

Following F03, the dynamic algorithm described here is tested against solutions of the steady isothermal multifluid equations. These steady-state equations are solved using an independent code, the details of which are outlined in Appendix C. The conditions for each of the tests are given in Table 1.

4.1 Case A: ambipolar dominated

In this test $r_{\mathrm{O}} = 2 \times 10^{-12}, r_{\mathrm{H}} = 1.16 \times 10^{-5}$ and $r_{\mathrm{A}} = 0.068$ giving $\eta = 5.86 \times 10^3$ and hence it can be expected that ambipolar diffusion will dominate the solution. Fig. 1 shows plots of the x-component of the neutral velocity, along with B_y for both the dynamic and steady-state solutions. The calculation shown has $h = 5 \times 10^{-3}$. It can be seen that the agreement between the two solutions is extremely good.

Since the algorithm is designed to be second order it is worthwhile measuring the convergence rate of the dynamic solution against the solution from the steady-state solver. The comparison is made by minimizing the L1 error norm, e_1, between a section of the dynamical solution and the steady-state solution. Working from the downstream side, the section $x_{\mathrm{L}} \leqslant x \leqslant x_{\mathrm{R}}$ is fixed about the point x^* where the deviation from the downstream state first exceeds 50 per cent of the maximum variation in the solution. Using $x_{\mathrm{L}} = x^* - 0.44$ and $x_{\mathrm{R}} = x^* + 0.56$ yields $e_1 = 3.90 \times 10^{-5}$ for
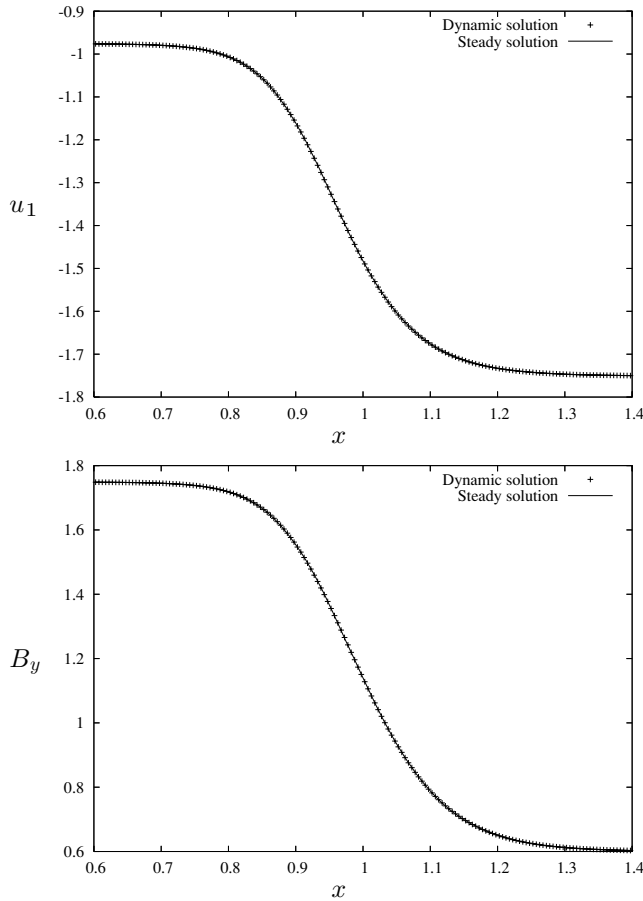
Figure 1. Neutral fluid *x*-velocity and *y*-component of magnetic field for case A with $h = 5 \times 10^{-3}$. The solution from the steady-state equations, as a line, is overplotted with points from the dynamic code.

$h = 5 \times 10^{-3}$, and $e_1 = 1.56 \times 10^{-4}$ for $h = 1 \times 10^{-2}$. This gives $e_1 \propto h^{2.0}$ – showing second-order convergence as expected.
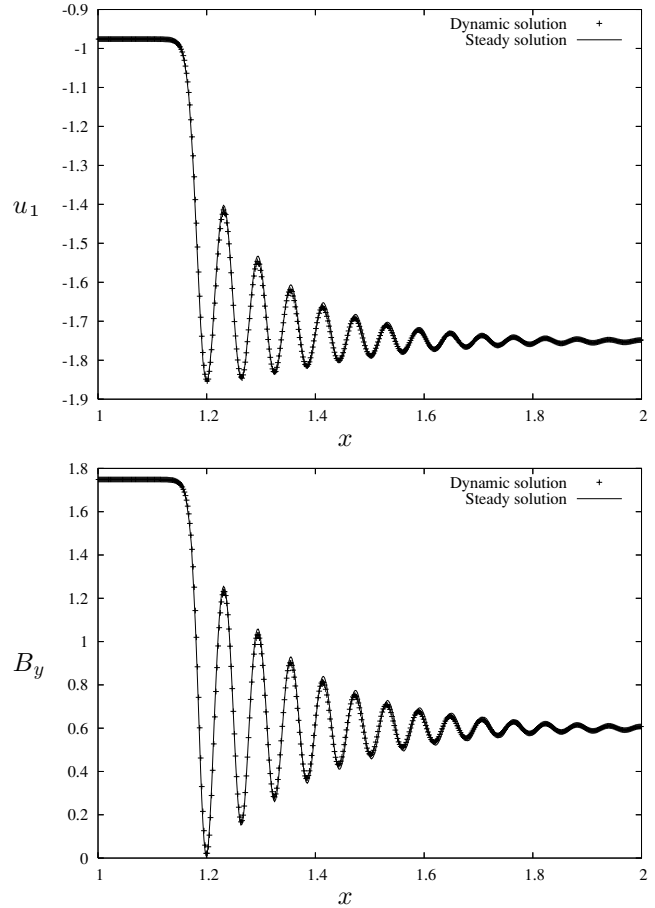
4.2 Case B: Hall dominated

The Hall term dominates in this test, requiring the Hall diffusion to be split and applied in part via HDS. The parameters are $r_O = 2 \times 10^{-9}$, $r_H = 0.0116$, $r_A = 5.44 \times 10^{-4}$ with $\eta = 0.0046$ $\ll 1$.[2] Fig. 2 shows the results of the calculations for the test with $h = 2 \times 10^{-3}$. For standard explicit codes the conditions lead to prohibitive restrictions on the time-step. However, the use of HDS allows us to maintain a time-step close to the Courant limit imposed by the hyperbolic terms throughout the calculations.

As with case A, the dynamic solution is tested to ensure it has the correct second-order convergence characteristics. With $x_L = x^* - 0.15$ and $x_R = x^* + 0.95$, we find $e_1 = 4.95 \times 10^{-3}$ for $h = 2 \times 10^{-3}$ and $e_1 = 1.15 \times 10^{-3}$ for $h = 1 \times 10^{-3}$, giving $e_1 \propto h^{2.1}$. Again, this is close to the second-order convergence rate expected.

4.3 Case C: neutral subshock

This test is similar to case A, but with a higher sound speed and upstream fast Mach number. As a result, a subshock develops in the

---

[2] If the Hall diffusion is increased much further, it appears that the approximation of negligible charged particle inertia breaks down.

Figure 2. Neutral fluid *x*-velocity and *y*-component of magnetic field for case B with $h = 2 \times 10^{-3}$. The solution from the steady-state equations, as a line, is overplotted with points from the dynamic code.

neutral flow because the interactions between the charged particles and the neutrals are not strong enough to completely smooth out the strong initial discontinuity in the neutral flow. The ability of the algorithm described to deal with discontinuities in the solution is therefore tested.

Fig. 3 shows the results of the calculations for $h = 1 \times 10^{-3}$. The subshock in the neutral flow is clearly visible as a discontinuity in u_1, while there is no corresponding discontinuity in B_y. Fig. 4 contains a plot of the *x*-component of the velocity of the negatively charged fluid. As expected, there is no discontinuity in this variable, but there are some oscillations at the point where the discontinuity in the neutral flow occurs. These errors are remarkably similar to those encountered by F03 and do not affect the global solution.

It can be expected that, since there is a discontinuity in the solution of this test, the rate of convergence of the dynamic solution will be close to first order, at least for resolutions high enough to discern the subshock in the solution. In this test $x_L = x^* - 0.13$ and $x_R = x^* + 0.15$. We find $e_1 = 3.41 \times 10^{-2}$ for $h = 5 \times 10^{-3}$ and $e_1 = 5.25 \times 10^{-3}$ for $h = 1 \times 10^{-3}$ yielding $e_1 \propto h^{1.16}$ – close to the first order expected, although clearly the error from around the subshock is not completely dominating at this resolution. At $h = 5 \times 10^{-4}$ we find $e_1 = 2.73 \times 10^{-3}$ giving $e_1 \propto h^{0.94}$ with respect to the error at $h = 1 \times 10^{-3}$. We suspect that the deviation from first order is due to a discontinuity in the electric field at the subshock causing an
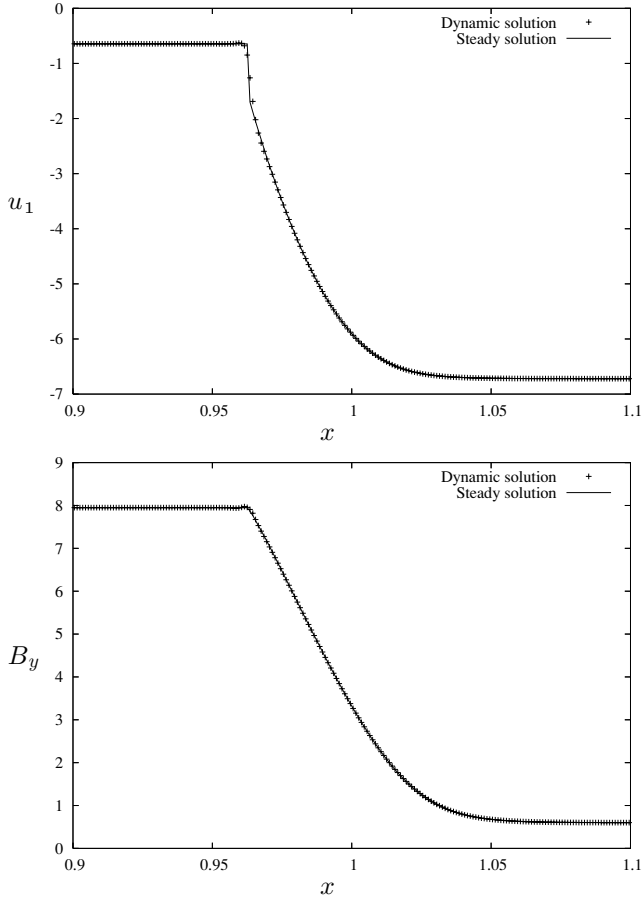
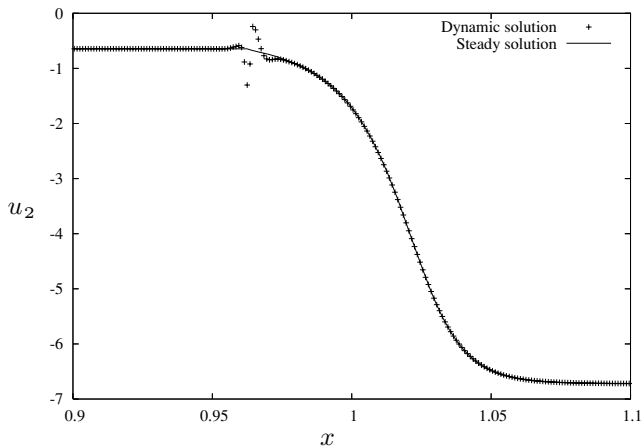**Figure 3.** Neutral fluid x-velocity and y-component of magnetic field for case C with $h = 1 \times 10^{-3}$. The solution from the steady-state equations, as a line, is overplotted with points from the dynamic code.

error in the charged velocities since smoothing the solution with some artificial viscosity is found to improve the convergence.

4.4 Comparative timings

In this section, comparison is made between the performances of standard explicit, STS/HDS and implicit (Crank–Nicolson) dis-

Figure 4. Negatively charged fluid x-velocity for case C with $h = 1 \times 10^{-3}$. The solution from the steady-state equations, as a line, is overplotted with points from the dynamic code.

Table 2. The speed-up factors in processor time usage achieved via the implicit and STS/HDS discretizations of the induction equation relative to the standard explicit discretization.

	Case A	Case B	Case C
STS/HDS	1.9	14.8	1.9
Implicit	1.9	23.3	2.7

cretizations of the induction equation. The different methods are applied in otherwise identical codes to the high-resolution trials of the preceding test cases. Since the neutral gas equations are treated explicitly in all cases, the corresponding Courant condition on the integration of the hyperbolic terms imposes a hard limit on the time-step.

As a benchmark, we use the standard explicit discretization sub-cycled to the same degree as the STS/HDS method. The speed-up factors of the STS/HDS and implicit methods in terms of processor time usage are presented in Table 2. Clearly, either technique offers a significant improvement in efficiency and both achieve time-steps close to the limit introduced by the hyperbolic terms. The implicit method is slightly faster for case C due to the high degree of sub-cycling used for the STS and significantly so for case B because of the very large Hall term. Otherwise, the STS/HDS and implicit methods yield similar speed-up factors indicating that overall efficiency is dominated by the other parts of the schemes. It should be emphasized that these are steady-state problems which suit implicit methods particularly well and for non-steady state problems accuracy constraints may reduce the efficiency of implicit schemes.

5 CONCLUSIONS

A new explicit scheme for integrating the multifluid equations in the limit of low ionization has been presented. The usual explicit stability limit imposed by the induction equation is relaxed by means of the STS algorithm applied for a portion of the Hall diffusion up to a critical limiting value.

Beyond this limiting value the standard explicit discretization becomes subject to a stability constraint requiring that the time-step vanish as the Hall diffusion becomes large. In order to circumvent this constraint, the excess Hall diffusion above the critical value is split off and applied via a new method which we have called HDS.

It has been demonstrated that, for the case of an isothermal flow, the algorithm is accurate and converges to second order when the solution is smooth and to first order when the solution contains a discontinuity. The extension of this scheme to non-isothermal flow does not present any obvious difficulties, although a modification of the discretization used for the magnetic flux evolution is necessary.

Since all discretizations used in the scheme presented here are explicit, it is a straightforward matter to implement in a multidimensional parallelized codes using AMR. This is a crucial advantage for large-scale simulations of astrophysical systems in which multifluid effects are thought to be important such as dense molecular clouds and protostellar accretion discs.

REFERENCES

Alexiades V., Amiez G., Gremaud P., 1996, Com. Num. Meth. Eng., 12, 31
Chieze J.-P., Pineau des Forets G., Flower D. R., 1998, MNRAS, 295, 672
Ciolek G. E., Roberge W. G., 2002, ApJ, 567, 947 (CR02)
Falle S. A. E. G., 1991, MNRAS, 250, 581
Falle S. A. E. G., 2003, MNRAS, 344, 1210 (F03)
Fendt C., Camenzind M., 1996, A&A, 313, 591
Ferreira J., 2004, Ap&SS, 293, 83
Hollerbach R., Rüdiger G., 2004, MNRAS, 347, 1273
Lery T., Heyvaerts J., Appl S., Norman C. A., 1999, A&A, 347, 1055
Ouyed R., Pudritz R. E., Stone J. M., 1997, Nat, 385, 409
Sano T., Stone J. M., 2002a, ApJ, 570, 314
Sano T., Stone J. M., 2002b, ApJ, 577, 534
Shu F., Najita J., Ostriker E., Wilkin F., Ruden S., Lizano S., 1994, ApJ, 429, 781
Smith M. D., Mac Low M.-M., 1997, A&A, 326, 801
Stone J. M., 1997, ApJ, 487, 271
Strang G., 1968, SIAM J. Numer. Anal., 5, 505
Tóth G., 1994, ApJ, 425, 171
Wardle M., 1991, MNRAS, 251, 119
Wardle M., 2004, Ap&SS, 292, 317

APPENDIX A: CHARGED VELOCITIES

For this work, the collisional coefficients K_{i1} are assumed to be independent of velocities and temperatures. The following derivation (S.A.E.G. Falle private communication) is included for completeness.

Transforming to the frame co-moving with the neutral gas, equation (5) can be written as

$$\boldsymbol{q}_i' \times \boldsymbol{B} - \kappa_i \boldsymbol{q}_i' = -\boldsymbol{E}' - \boldsymbol{q}_1 \times \boldsymbol{B}, \qquad (A1)$$

where $\kappa_i \equiv \rho_1 K_{i1}/\alpha_i$ and $\boldsymbol{E}' = \boldsymbol{E} + \boldsymbol{q}_1 \times \boldsymbol{B}$.

Then choosing $i = 2$ as a reference species, the general solutions for velocities of the remaining charged species are given by

$$\boldsymbol{q}_i' = \mathbf{A}_i^{-1} \mathbf{A}_2 \boldsymbol{q}_2', \qquad (A2)$$

where

$$\mathbf{A}_i = \begin{pmatrix} -\kappa_i & B_z & -B_y \\ -B_z & -\kappa_i & B_x \\ B_y & -B_x & -\kappa_i \end{pmatrix}. \qquad (A3)$$

To derive the charged velocities, all that remains is for the reference velocity to be evaluated, this can be done by using equation (9) and Ampère's law to give

$$\boldsymbol{q}_2' = \left[\mathbf{I} - \left(\sum_{i=3}^{N} \frac{\alpha_i \rho_i}{\alpha_2 \rho_2} \mathbf{A}_i^{-1} \right) \mathbf{A}_2 \right]^{-1} \frac{\nabla \times \boldsymbol{B}}{\alpha_2 \rho_2}. \qquad (A4)$$

If the collisional coefficients are in fact dependent on the velocities of the charged species, this procedure can be carried out iteratively using the values from the previous time-step as a starting point.

Should the collisional coefficients depend on the temperatures of the charged species, some additional calculation is necessary before the next iteration: using equation (6) and inserting the specific form

of the function G_{i1}, $N - 1$ equations are obtained which may be solved readily for the $N - 1$ charged temperatures.

Finally, it is worth noting that superior results are obtained by interpolating the primitive quantities to the cell edges before calculating the charged velocities rather than by calculating the velocities at the cell centres and interpolating from these to the edges.

APPENDIX B: HALL DIFFUSION SCHEME IN THREE DIMENSIONS

Equation (5) can be used in conjunction with equation (9) to write the electric field for pure Hall diffusion as

$$\boldsymbol{E} = r_{\mathrm{H}} \frac{\boldsymbol{J} \times \boldsymbol{B}}{B}. \qquad (B1)$$

Then, using Faraday's law, we can write

$$\frac{\partial \boldsymbol{B}}{\partial t} = -\nabla \times (r_{\mathrm{H}} \boldsymbol{J} \times \boldsymbol{b}), \qquad (B2)$$

where $\boldsymbol{b} \equiv \boldsymbol{B}/B$.

This equation can be expanded out and linearized to give

$$\frac{\partial \boldsymbol{B}}{\partial t} = \mathbf{G}\boldsymbol{B}, \qquad (B3)$$

where, using $\boldsymbol{J} = \nabla \times \boldsymbol{B}$, the matrix operator $\mathbf{G}$ is given by

$$\mathbf{G} = -r_{\mathrm{H}}(\boldsymbol{b} \cdot \nabla)\nabla \times . \qquad (B4)$$

Hence $\mathbf{G}$ is antisymmetric and we can write the generalized HDS scheme as

$$B_x^{n+1} = B_x^n + \tau \left(G_{xy}^n B_y^n + G_{xz}^n B_z^n \right), \qquad (B5)$$

$$B_y^{n+1} = B_y^n + \tau \left(G_{yz}^n B_z^n + G_{yx}^n B_x^{n+1} \right), \qquad (B6)$$

$$B_z^{n+1} = B_z^n + \tau \left(G_{zx}^n B_x^{n+1} + G_{zy}^n B_y^{n+1} \right), \qquad (B7)$$

where $\mathbf{G}^n$ is the discretized form of the matrix operator $\mathbf{G}$ at time level n.

The generalized HDS scheme in three dimensions is analogous in construction to the one-dimensional case in that equation (B5) is an explicit first step and equation (B7) is an implicit-like final step. Additionally, we now have an intermediate step of mixed explicit/implicit character. Numerical tests indicate that the method retains its favourable stability properties in three dimensions.

APPENDIX C: STEADY-STATE SOLVER

Assuming an isothermal flow, as is the case for the tests presented in this work, setting all derivatives with respect to time to zero in the multifluid equations gives us

$$\rho_i u_i = Q_i = \text{constant}, \qquad (C1)$$

$$\rho_1 u_1^2 + a^2 \rho_1 + \frac{B^2}{2} = P_x = \text{constant}, \qquad (C2)$$

$$\rho_1 u_1 v_1 - B_x B_y = P_y = \text{constant}, \qquad (C3)$$

$$\rho_1 u_1 w_1 - B_x B_z = P_z = \text{constant}. \qquad (C4)$$

In addition the reduced momentum equations for the charged species (equation 5) yield three equations for each charged species, and the

charge neutrality condition is also used. Finally, the equation for $\boldsymbol{B}$ yields

$$\boldsymbol{M} - \boldsymbol{M}_{\mathrm{R}} = \mathbf{R}\frac{\mathrm{d}\boldsymbol{B}}{\mathrm{d}x} \qquad (\mathrm{C5})$$

with $\boldsymbol{M}_{\mathrm{R}}$ ($=\boldsymbol{M}_{\mathrm{L}}$) being the flux in the right (left) state.

For the cases considered here, with two charged species, the above equations constitute one ordinary differential equation for $\boldsymbol{B}$ and seven equations which, once $\boldsymbol{B}$ is known at a given point in space, can be used to solve for all the other variables. The ordinary differential equation (ODE) for $\boldsymbol{B}$ is solved using the Runge–Kutta method of order 4.

The initial conditions (at $x = 0$) are a saddle point of the ODE for $\boldsymbol{B}$. These conditions are perturbed slightly and the system then evolves through phase space to a sink point.

This paper has been typeset from a TEX/LATEX file prepared by the author.